INSTITUTE OF PHYSICS PUBLISHING JOURNAL OF PHYSICS: CONDENSED MATTER

J. Phys.: Condens. Matter **16** (2004) 6763–6769 PII: S0953-8984(04)83107-2

High-temperature phase transitions in $SrBi_2Ta_2O_9$ film: a study by THz spectroscopy

F Kadlec, S Kamba, P Kužel, C Kadlec, J Kroupa and J Petzelt

Institute of Physics, Academy of Sciences of the Czech Republic, Na Slovance 2, 182 21 Prague 8, Czech Republic

Received 25 June 2004, in final form 11 August 2004
Published 3 September 2004
Online at stacks.iop.org/JPhysCM/16/6763
doi:10.1088/0953-8984/16/37/012

Abstract

A time-domain THz transmission experiment was performed on a $SrBi_2Ta_2O_9$ film deposited on a sapphire substrate. Temperatures between 300 and 923 K were investigated and complex permittivity spectra of the film were determined. The lowest-frequency optical phonon near 28 cm^{-1} reveals a slow monotonic decrease in frequency on heating with no significant anomaly near the phase transitions. We show that the dielectric anomaly near the ferroelectric phase transition can be explained by the slowing down of a relaxational mode, observed in the THz spectra. A second-harmonic generation signal observed for a single crystal confirms the loss of a centre of symmetry in the ferroelectric phase and the presence of polar clusters in the intermediate ferroelastic phase.

1. Introduction

Although ferroelectricity in $SrBi_2Ta_2O_9$ (SBT) was already discovered at the beginning of the 1960s [1, 2], this material was intensively investigated mainly only in the last decade; the motivation for the study comes from its excellent polarization fatigue-free behaviour, low leakage currents and the possibility of depositing extremely thin films without loss of bulk characteristics [3]. These properties allowed the use of SBT films in commercial non-volatile ferroelectric memories. On the other hand, the structural phase transitions (PTs) in SBT are still not well characterized.

SBT crystallizes in the so-called Aurivillius structure, where the perovskite-type groups $[SrTa_2O_7]^{2-}$ and $[Bi_2O_2]^{2+}$ layers are stacked alternately along the pseudotetragonal c axis [4, 5]. At room temperature the Bi_2O_2 layers and TaO_6 octahedra are considerably distorted and atomic displacements along the a axis give rise to spontaneous polarization [6]. The ferroelectric phase has the space group $A2_1am$ ($Z_{prim} = 2$) and the structure undergoes a PT to a paraelectric phase at T_{c1} near 600 K. Recently, it was discovered that this tetragonal phase ($Amam$ space group, $Z_{prim} = 2$) [7–9] is ferroelastic and that, at $T_{c2} \approx 770$ K, the compound undergoes another PT to a phase with the $I4/mmm$ ($Z_{prim} = 1$) space

group symmetry. The latter PT is improper ferroelastic (with doubling of the primitive unit-cell volume on cooling) while the former one is proper ferroelectric (no multiplication of the primitive unit-cell volume with respect to the ferroelastic phase) [9].

The dynamics of the PTs in SBT was investigated first by means of Raman scattering [10–13] and later by means of Brillouin scattering [14] and Fourier transform infrared (FTIR) reflectivity and transmission spectroscopy [9, 15, 16]. It was shown that the lowest-frequency optical phonon near 28 cm^{-1} (at 300 K) reduces its frequency on heating and disappears from the Raman spectra above T_{c1} due to overdamping and the change of selection rules [10]. Therefore this mode was called an optical soft mode. However, high-temperature FTIR transmission spectra revealed its weak monotonic softening down to 20 cm^{-1} at 950 K with no significant anomaly near either T_{c1} or T_{c2} [16]. Such a behaviour cannot explain the dielectric anomaly observed in low-frequency dielectric data near T_{c1}; therefore the name soft mode is not fully justified. Kamba *et al* [9] proposed the existence of an additional relaxational mode, which would slow down near T_{c1} and induce the corresponding dielectric anomaly. Indeed, this relaxation was recently observed by time-domain THz spectroscopy (TDTS) below 300 K [16, 17].

The present paper reports high-temperature TDTS experiments using the same SBT film sample as in [16], as well as second-harmonic generation (SHG) data from a SBT single crystal, with the aim of studying the mechanism of the two phase transitions. At the same time, for high-temperature measurements, the THz spectroscopy as a time-domain method using gated detection has been supposed to present clear advantages over FTIR measurements [18]. To our knowledge, this is the first report of TDTS measurements in a furnace, confirming the suitability of the method for such experiments.

2. Experimental details

The same SBT polycrystalline film (thickness 5.5 μm) and TDTS set-up as described in the previous work [16] were used. For sample heating, we used an adapted commercial high-temperature cell (SPECAC P/N 5850) with 1 mm thick sapphire windows. The measurements were performed in a closed experimental chamber which was evacuated and re-filled with dry nitrogen in order to ensure temperature homogeneity around the sample. A supplementary external cooling circuit was used to remove the excess heat from the chamber. For each temperature, complex transmittance spectra of both the film on the substrate and a reference sapphire substrate were measured.

The second-harmonic generation (SHG) signal was measured for a SBT single crystal with dimensions of about $2 \times 1 \times 0.1$ mm^3, its large face being perpendicular to the c axis. The same crystal was used in previous studies [9, 15]. A Q-switched Nd-YAG laser served as a light source. The pulse energy was 0.2 mJ and the beam was only slightly focused ($2w \approx 300$ μm) on the sample. After filtering the fundamental frequency, the SHG signal was detected by a photomultiplier connected to a boxcar integrator (PAR 162). The sample was placed in a custom-made heating cell and the temperature was continuously swept with a rate of 5 K min^{-1} up to 900 K. It was possible to monitor the position of the beam on the sample in the oven.

3. Results and discussion

The complex dielectric spectra of SBT thick film at various temperatures are shown in figure 1. The spectra were fitted with a sum of two damped Lorentz oscillators (describing the polar phonons) and a Debye relaxation accounting for the central mode (CM):

$$\varepsilon^*(\omega) = \varepsilon'(\omega) + \mathrm{i}\varepsilon''(\omega) = \frac{\Delta\varepsilon_\mathrm{r}\omega_\mathrm{r}}{\omega_\mathrm{r} + \mathrm{i}\omega} + \sum_{j=1}^{2} \frac{\Delta\varepsilon_j\omega_j^2}{\omega_j^2 - \omega^2 + \mathrm{i}\omega\gamma_j} + \varepsilon_\infty \qquad (1)$$

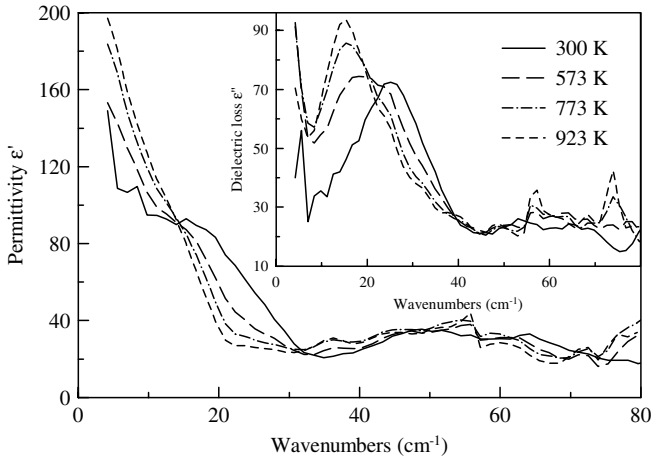

Figure 1. Experimental real and imaginary parts of the complex THz permittivity in SBT plotted at various temperatures. Features near 57 and 73 cm^{-1} are due to residual water vapour absorption.

where ω_r and $\Delta\varepsilon_r$ are the relaxation frequency and dielectric strength of the CM, respectively; ω_j, γ_j and $\Delta\varepsilon_j$ denote the eigenfrequencies, damping and contribution to the static permittivity from the jth polar phonon mode, respectively, and ε_∞ describes the high-frequency permittivity originating from the electronic polarization and from the polar phonons above 80 cm^{-1}. For each temperature, we have found such a set of parameters that the resulting $\varepsilon^*(\omega)$ matches the experimental data. As in the case of the low-temperature spectra [16], the shape of the spectra in the low-frequency part strongly indicates the presence of a relaxational mode. However, it is important to note that its frequency ω_r is lower than the experimental limit of the experiment. Therefore, it is not possible to unambiguously determine its parameters from the experimental data alone. When deducing the parameters to employ in equation (1), we have kept the relaxation strength $\Delta\varepsilon_r\omega_r$ constant and varied the value of $\Delta\varepsilon_r$ so as to describe the dielectric anomaly at T_{c1} [19]. The resulting functions $\varepsilon^*(\omega)$ describe our experimental data very well over the whole temperature range studied.

As an example, the experimental spectrum of ε^* at $T = 573$ K and the fitted curves are shown in figure 2. Two calculated functions $\varepsilon^*(\omega)$ are shown—with and without the relaxational CM. Both sets of curves satisfactorily describe ε^* above 15 cm^{-1}; however, the model without the CM yields a worse agreement in the low-frequency part of the spectra and, above all, it leads to a value of the static permittivity ε_0 which is too low ($\approx$130 near T_{c1}). Although the accuracy of our data below 10 cm^{-1} is limited, the curves with the CM clearly describe the experimental spectra much better and are compatible with the dielectric anomaly near T_{c1}.

The temperature dependences of the eigenfrequencies of the CM and of the lowest-frequency phonon together with their dielectric strengths are shown in figure 3. In the spectra simulations, the CM exhibits a slowing down to T_{c1} and a frequency increase at higher temperatures. The first phonon exhibits no anomaly—only a slow decrease of its eigenfrequency $\Delta\omega_1$ with temperature and an increase of the dielectric strengths $\Delta\varepsilon_1$ were observed. In conclusion, we find that only the CM can explain the dielectric anomaly near the ferroelectric PT at T_{c1}.

Note that the values of the permittivity maximum ε'_{max} at T_{c1} reported by various authors are different and range from 280 [1] to 580 [2] for stoichiometric ceramics. In the case of nonstoichiometric $Sr_{1\pm x}Bi_{2\pm y}Ta_2O_9$ ceramics, ε'_{max} can be even higher, but T_{c1} also rises [19].

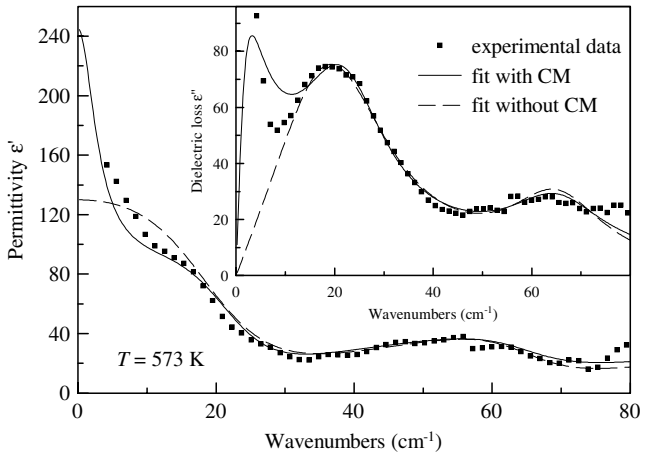

Figure 2. Experimental THz dielectric spectra at 573 K together with different fits (see the text for details).

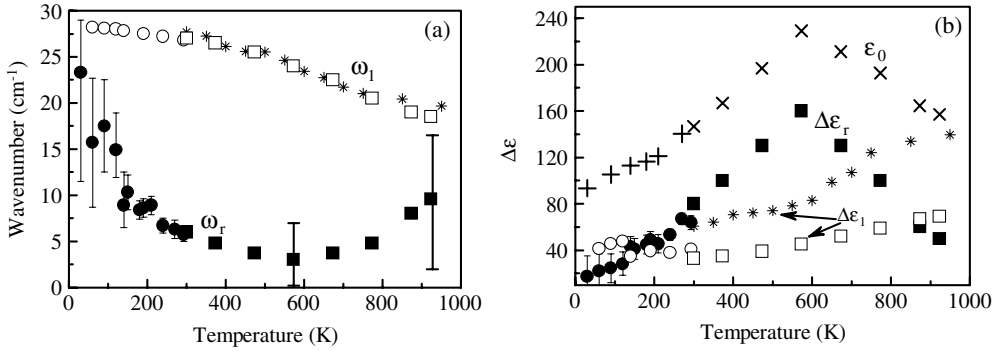

Figure 3. (a) Temperature dependences of frequencies of the CM ω_r and of the first optical phonon ω_1. The stars result from fits of FTIR transmittance measurements [20]. (b) Temperature dependences of dielectric strengths of the CM ($\Delta\varepsilon_r$, full symbols) and of the lowest-frequency phonon ($\Delta\varepsilon_1$). Open symbols denote $\Delta\varepsilon_1$ obtained from the fit with the CM, stars come from oscillator fit of FTIR spectra without the CM. The temperature dependence of the static permittivity ε_0 is also shown. The symbols below 300 K are taken from previously published TDTS data [16].

On the other hand, it is known that ε' for SBT is size dependent only for films with thickness less than 200 nm, which is much less than the 5.5 μm of our case. The static permittivity resulting from our TDTS experiment is somewhat lower than the value published for ceramics. This can be explained by cracks and fine scratches in the film which we observed using a microscope. The TDTS is sensitive to the in-plane permittivity of the film and the cracks can strongly reduce the dielectric response [20]. The room temperature THz spectra of the SBT film have been measured several times during the last two years and it was found that the dielectric function in the THz range decreased with time (compare e.g. figure 1 in [16] and that in the present paper). This is apparently due to the increasing concentration of scratches and/or cracks in our film following the mechanical and thermal handling of the sample.

By contrast, the sample age had no influence on the phonon frequencies. Figure 3 shows the temperature dependence of ω_1 obtained from the TDTS and FTIR transmission [20] spectra; the agreement between the two is excellent. The FTIR transmission spectra were fitted without

Table 1. Factor-group analysis of the three phases of SBT. The assignment of the mode activities is explained in the text. Note that the x and y axes in the tetragonal phase are 45° rotated with respect to those of the low-temperature phases.

$A2_1am$ (C_{2v}^{12})	$Amam$ (D_{2h}^{17})	$I4/mmm$ (D_{4h}^{17})
22 $A_1(x, x^2, y^2, z^2)$	11 $A_g(x^2, y^2, z^2)$	4 $A_{1g}(x^2 + y^2, z^2)$
	11 $B_{3u}(x)$	8 $E_u(x, y)$
22 $B_2(y, xy)$	14 $B_{2u}(y)$	
	8 $B_{1g}(xy)$	2 $B_{1g}(x^2 - y^2)$
20 $A_2(yz)$	6 $A_u(-)$	1 $B_{2u}(-)$
	14 $B_{3g}(yz)$	6 $E_g(xz, yz)$
20 $B_1(z, xz)$	9 $B_{2g}(xz)$	
	11 $B_{1u}(z)$	7 $A_{2u}(z)$

the CM; therefore its dielectric strength $\Delta\varepsilon_1$ is also higher than that obtained from the TDTS with the CM taken into account. The oscillator fits of THz spectra without the CM yield dielectric strengths in agreement with the fits in [16], so the different values in figure 3 are not due to the different experimental methods but due to the different fitting procedures. Let us stress that our data confirm that the lowest-frequency phonon displays no anomaly in ω_1 near T_{c1} or T_{c2} which implies that this mode does not drive the ferroelectric PT.

Stachiotti *et al* [21] studied the lattice dynamics in SBT using the frozen-phonon approach and proposed a soft mode of E_u symmetry (assignment in the paraelectric $I4/mmm$ structure), which involves a vibration of Bi atoms relative to the TaO_6 perovskite-like blocks. However, the freezing of the polar E_u mode does not lead to the observed ferroelectric phase of $A2_1am$ symmetry nor to an intermediate ferroelastic phase. Perez-Mato *et al* [22] studied the stability of phases in SBT by means of *ab initio* calculations and came to the conclusion that two unstable modes are responsible for the two subsequent phase transitions. The stronger instability relates to the X_3^- nonpolar mode (this mode from the X point of the Brillouin zone involves antiphase tilting of TaO_6 octahedra), the freezing of which leads to the $Amam$ intermediate phase with a doubled unit cell. The subsequent condensation of the E_u polar mode is responsible for the $A2_1am$ ferroelectric phase. Perez-Mato *et al* [22] also showed that another very hard secondary nonpolar mode of X_2^- symmetry involving only a vibration of oxygen atoms within the Bi_2O_2 layers is in fact essential for the final stabilization of the ferroelectric phase. From our data it follows that the E_u soft mode is not a phonon but rather a relaxational mode corresponding possibly to an anharmonic vibration of Bi ions at the Sr sites (anti-site defects are known to exist in SBT [7]). The X_3^- mode can become Raman active below T_{c2}; however this mode was not observed in the ferroelastic phase, because Raman experiments were performed only below T_{c1} [10, 11].

The factor-group analysis for all three crystal phases is shown in table 1. The activities of the modes in the spectra are shown in parentheses. The modes active in the infrared spectra with the electrical field parallel to the crystal axes are denoted by x, y, z while x^2, y^2, z^2, xy, xz and yz signify the elements of the symmetric Raman tensor. The table allows us to assign the modes in the THz spectra. The relaxational soft mode drives the ferroelectric PT, so in the three phases it displays the symmetries E_u, B_{3u} and A_1 as the temperature is decreased. The hard mode near 55 cm^{-1} was not observed in the FTIR reflectivity spectra of a (001) oriented single crystal [9], where only $E \parallel x, y$ modes were active, unlike in the spectra of ceramics

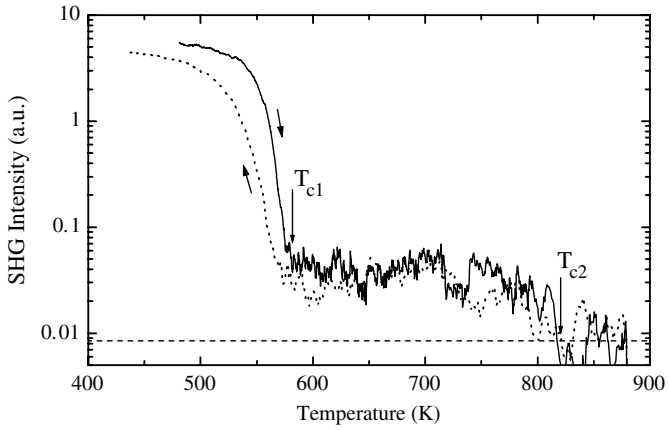

Figure 4. The temperature dependence of the SHG signal for SBT single crystal for parallel polarizations on heating and cooling. The noise limit is marked by the dashed curve.

and thick film. Therefore, in the three phases, it has the symmetry A_{2u}, B_{1u}, B_1. The lowest-frequency phonon (near 28 cm^{-1} at $T \rightarrow 0$ K) has the E_u symmetry, but its assignment at low temperatures is ambiguous—it can have either an A_1 or a B_2 symmetry in the ferroelectric phase. The symmetry could be unambiguously determined only by means of Raman scattering investigation of a single-domain SBT crystal. Nevertheless, it follows from table 1 that all doubly degenerate E_u modes (both the relaxational CM as well as the mode near 28 cm^{-1}) should split into two components in the orthorhombic phase and both components should be active in our spectra. However, we do not see any splitting, which means that the splitting is probably very small or one of the components is very weak. The third possible explanation, that the second component appears above our frequency range, is highly unlikely because our previous FTIR transmission measurements [16] do not reveal any new mode below T_{c2} in the frequency range up to 150 cm^{-1}. Let us note that table 1 can also be useful for interpretation of further high-temperature FTIR and Raman spectra of SBT and other Aurivillius compounds with an intermediate phase.

Figure 4 shows the temperature dependence of the SHG signal from the SBT single crystal. A strong SHG signal is seen in the ferroelectric phase below T_{c1} confirming the absence of a centre of symmetry. This signal was independent of the polarization of the incident and generated beams. Between T_{c1} and T_{c2}, the signal is two orders of magnitude lower, but still one order of magnitude higher than the noise level. The SHG signal in the ferroelastic phase was detected only for the polarization parallel to that of the incident beam; surprisingly, no SHG was observed for the perpendicular polarization. The small SHG signal indicates the presence of polar clusters in the ferroelastic phase. Above T_{c2}, the SHG signal is zero within the accuracy of our experiment. This supports the picture according to which the instability in the high-temperature tetragonal phase appears only (or prevailingly) at the X point of the Brillouin zone (the X_3^- irreducible representation [22]). The ferroelectric instability is then triggered by the freezing of the X_3^- mode in the ferroelastic phase, mainly due to a trilinear coupling term in the free-energy expansion involving soft X_3^- and E_u coordinates and a hard X_2^+ coordinate, as shown by Perez-Mato *et al*. The polar clusters in the ferroelastic phase account then for the ferroelectric fluctuations and permittivity increase and their dynamic manifestation could be the CM revealed in our experiment. This situation reminds us of that of relaxor ferroelectrics in which the appearance of polar clusters—including their strong CM-

type dielectric dispersion—is connected with the so-called Burns temperature (analogous to T_{c2}). By analogy with this picture we could expect the CM to disappear from the spectra above T_{c2}; this might be compatible with our data, which have, below 10 cm^{-1} and at high temperatures, only a limited accuracy.

4. Conclusion

THz dielectric spectra of SBT taken at temperatures up to 923 K confirm our previous results [9] obtained by means of FTIR transmission spectroscopy. On heating, the lowest-frequency phonon near 28 cm^{-1} exhibits a slow continuous decrease in frequency without any anomaly near either of the phase transitions. This implies that this mode does not drive any phase transitions. The earlier proposed relaxation mode [9] was observed in the THz spectra. We have shown that the assumption of its slowing down to T_{c1} is in agreement both with the THz spectra obtained experimentally and with the dielectric anomaly near the ferroelectric PT. The SHG signal was observed not only in the ferroelectric phase, but also weakly in the centrosymmetric ferroelastic phase, which gives evidence of the presence of polar clusters in this phase.

Acknowledgments

The work was supported by the Czech Academy of Sciences (projects Nos A1010213, AVOZ01-010-914 and K1010104) and the Grant Agency of the Czech Republic (project No 202/04/0993). The financial support of the Ministry of Education of the Czech Republic (project No LN00A032) is also acknowledged. The authors thank A Garg and Z H Barber for providing an excellent SBT film.

References

[1] Smolenskii A G, Isupov V and Agranovskaya A I 1961 *Sov. Phys.—Solid State* **3** 651
[2] Subbarao E 1962 *J. Phys. Chem. Solids* **23** 665
[3] Scott J 1998 *Ferroelectr. Rev.* **1** 1
[4] Newnham R, Wolfe R, Horsey R, Diaz-Colon F and Kay M I 1973 *Mater. Res. Bull.* **8** 1183
[5] Rae A D, Thompson J G and Withers R L 1992 *Acta Crystallogr.* B **48** 418
[6] Shimakawa Y, Kubo Y, Nakagawa Y, Kamiyama T, Asano H and Izumi F 1999 *Appl. Phys. Lett.* **74** 1904
[7] Macquart R, Kennedy B J, Kubota Y, Hishibori E and Takata M 2000 *Ferroelectrics* **248** 27
[8] Hervoches C H, Irvine J T S and Lightfoot P 2001 *Phys. Rev.* B **64** 100102
[9] Kamba S, Pokorny J, Porokhonskyy V, Petzelt J, Moret M P, Garg A, Barber Z and Zallen R 2002 *Appl. Phys. Lett.* **81** 1056
[10] Kojima S 1998 *J. Phys.: Condens. Matter* **10** L327
[11] Kojima S and Saitoh I 1999 *Physica* B **263/264** 653
[12] Ching-Prado E, Pérez W, Reynéz-Figueroa A, Katiyar R S and Desu S B 1999 *Ferroelectr. Lett.* **25** 53
[13] Ching-Prado E, Pérez W, Reynéz-Figueroa A, Katiyar R S, Ravichandran D and Bhalla A S 1999 *Ferroelectr. Lett.* **25** 97
[14] Ko J H, Hushur A and Kojima S 2002 *Appl. Phys. Lett.* **81** 4043
[15] Moret J P, Zallen R, Newnham R E, Joshi P and Desu S B 1998 *Phys. Rev.* B **57** 5715
[16] Kempa M, Kužel P, Kamba S, Samoukhina P, Petzelt J, Garg A and Barber Z H 2003 *J. Phys.: Condens. Matter* **15** 8095
[17] Kužel P, Pashkin A, Kempa M, Kadlec F, Kamba S and Petzelt J 2004 *Ferroelectrics* **300** 125
[18] Han P Y, Tani M, Usami M, Kono S, Kersting R and Zhang X C 2001 *J. Appl. Phys.* **89** 2357
[19] Kim J S, Cheon C, Shim H S and Lee C L 2001 *J. Eur. Ceram. Soc.* **21** 1295
[20] Rychetský I, Petzelt J and Ostapchuk T 2002 *Appl. Phys. Lett.* **81** 4224
[21] Stachiotti M G, Rodriguez C O, Ambrosh-Draxl C and Christensen N E 2000 *Phys. Rev.* B **61** 14434
[22] Perez-Mato J M, Blaha P, Parlinski K, Schwarz K, Aroyo M, Elcoro L and Izaola Z 2004 *Phys. Rev.* B submitted